

EXPERIMENTAL INVESTIGATION OF GEOMETRICAL EFFECT ON FLOW AND HEAT TRANSFER PERFORMANCE OF LAMILLOY COOLING STRUCTURE

by

Bo ZHANG*, Libing LIN, Naru ZHANG, Shuangsong XUE, and Honghu JI

Jiangsu Province Key Laboratory of Aerospace Power System, College of Energy and Power,
Nanjing University of Aeronautics and Astronautics, Nanjing, China

Original scientific paper
<https://doi.org/10.2298/TSCI190528071Z>

Effect of film hole diameter to discharge coefficients and film cooling effectiveness of the lamilloy were experimentally investigated at the blowing ratios ranging from 0.6 to 2.5. Generally, the cooling effectiveness on the test surface is increased with the film hole diameters and blowing ratios increasing, and the variation tendency along the streamwise through the centerline of film holes also keeps consistent. In the upstream, all configurations have a relatively lower cooling effectiveness, however, with the flows to the downstream, cooling effectiveness grows gradually, and the peak values of effectiveness appeared periodically, the position matches the film hole positions. Besides, between the film holes, fluctuation exists simultaneously. By comparison, the cooling effectiveness and discharge coefficients are both increased with the blowing ratio with same film hole diameters. Moreover, under the same blowing ratios, the cooling effectiveness and discharge coefficients are getting higher when hole diameters increase.

Key words: lamilloy, heat transfer, discharge coefficients, combustor, film cooling

Introduction

Demands for increased the propulsion thrust and the thermal efficiency of aero engine, caused the engine designers to increase combustion exit gas temperature, so that the turbine inlet temperature was continuously raised and has been higher than the melting point of the metal material used in the engines. Therefore, cooling the exposed combustor and downstream turbine surfaces has subsequently become a critical issue because of increased thermal loads and the cooling technique must be used to guarantee the work of engine. Clearly, there is a goal of film-cooling engine designers to reduce the amount of coolant used, while at the same time increasing the cooling efficiency. The lamilloy, which has the structure of jet impingement and the pin-fins inside, has a highly cooling effectiveness.

The lamilloy cooling technology was initially applied to the thermal protection of the combustor. The Allison company developed *lamilloy*, a cooling structure composed of three layers, in which the pin-fins are between the cavity. The flexibility, process complexity, cooling effectiveness and durability were studied systematically and the different types of combustor has been tested, results show the cooling efficiency can reach 0.7-0.9 [1-5]

* Corresponding author, e-mail: zhangbo_pe@nuaa.edu.cn

The measurement of temperature is crucial in the heat transfer performance of the lamilloy, and the non-contact technology is a reliable method for the description of the internal heat transfer coefficient distributions. Sweeney *et al.* [6] used the infrared thermal imaging technology to make detailed, 2-D steady-state measurements of flat plate surface temperature. Kong *et al.* [7] obtained the heat transfer coefficient distribution on the target surface, the impingement surface and the pin-fin surface of the large-scale lamilloy by the transient liquid crystal thermography. Funazaki *et al.* [8, 9] applied the narrow banded thermochromatic liquid crystal (TLC) technology to determine the heat transfer characteristics of the lamilloy with different internal geometric parameters and obtained the optimal one. Wu *et al.* [10] investigated the porous triple-laminated plate, results show that violent impingement and turbulent flow inside the plate contribute greatly to local heat transfer intensification. Zhang *et al.* [11] studied the heat transfer in impingement and film composite cooling structure of combustion chamber, and found stage-shaped holes formed impact inside the wall, tapped the coolant potential in cooling, and increased the heat transfer inside the solid. Andrews *et al.* [12] investigated the heat transfer characteristics of rectangular pin-fins array on the lamilloy cooling structure.

Experimental apparatus and procedure

Experimental apparatus

Figure 1 shows a schematic of the overall experiment system. The mainstream passes the blower and burns in the combustor, then flows through the valves, vortex flowmeter and contraction section before enters the grilles that ensure a uniform flow enters the test channel. The coolant air provided by centrifugal air blower passes through the air tank, valve, vortex flowmeter and contraction section, finally enters the chamber. In the experimental proceed, the main flow kept as constant, while the coolant was adjusted flow rate to the different blow ratio. Infrared thermography system was used to measure the surface temperature, T_w , in the experiment, which was calibrated by five *K*-type thermocouples, as shown in fig. 2, the 2(b) is the top view of the 2(a), the operation conditions are listed in the tab. 1, which also shows the six blowing ratios studied in this paper.

In the experiment, the flow rate of coolant was controlled by valve to reach the blowing ratio verifying from 0.6 to 2.5. The micro-pressure gauge installed in the mainstream channel is used to get the static pressure through the pressure pipe. The fig. 2 gives the pres-

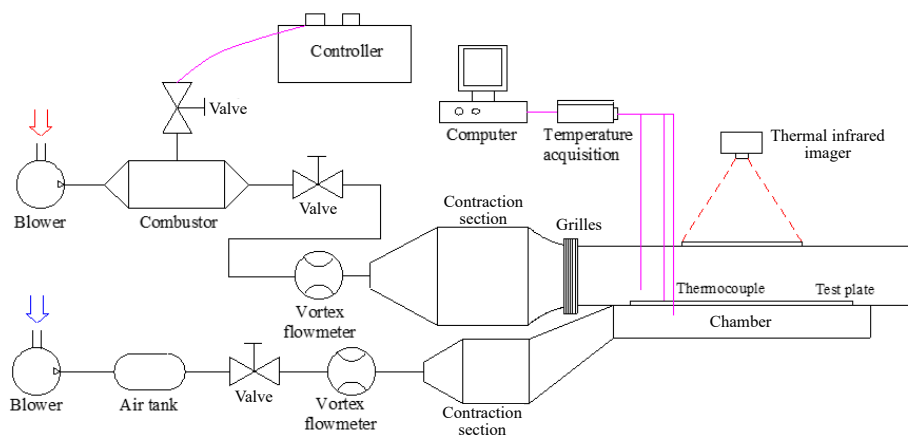


Figure 1. Sketch of the experiment system

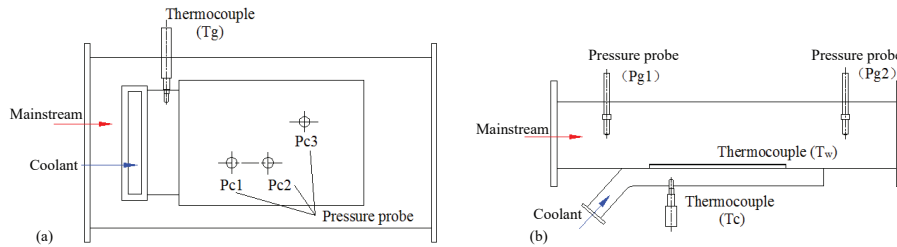


Figure 2. Thermocouple and pressure probe in the test system

sure probes installation in the test system, two probes placed near the inlet and outlet separately to get the value of P_{g1} and P_{g2} , and the average pressure is the static pressure P_g . Three probes are placed as fig. 2(a) to measure the coolant pressure $P_c^* = (P_{c1} + P_{c2} + P_{c3})/3$. Therefore, the discharge coefficient is the ratio of real mass-flow rate to ideal mass-flow defined by assuming isentropic, 1-D expansion across the hole from coolant total pressure to main flow static pressure level.

Lamilloy cooling configurations

The configuration of the lamilloy tested in the experiments is shown in fig. 3. It consists of jet plate with one converted impingement holes (the blue shaded hole) whose diameter is 0.65 mm, a target plate with one converted film holes (the red shaded hole), and four Pin-fins whose diameter is 1 mm in a unit shown as dotted lines. The test plates features 245×200 mm cross-section and the holes area is $150 \text{ mm} \times 100 \text{ mm}$ on the plate. All the lamilloy material is stainless steel. Four configurations investigated in this paper are shown in tab. 1.

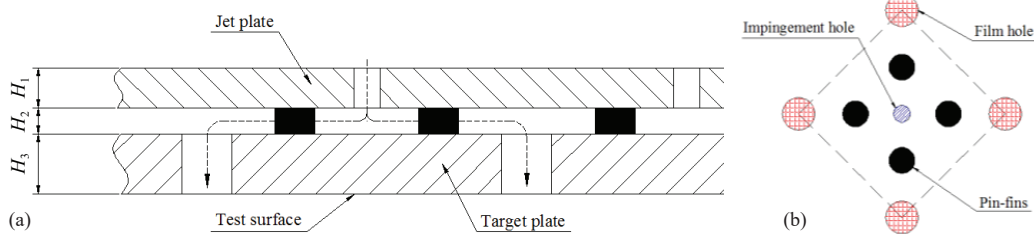


Figure 3. Schematic of the lamilloy

Table 1. Lamilloy parameters investigated

Configuration	H_1	H_2	H_3	d_i	d_p	d_f [mm]
A	1	0.65	1.5	0.65	1	0.65
B	1	0.65	1.5	0.65	1	0.85
C	1	0.65	1.5	0.65	1	1.05
D	1	0.65	1.5	0.65	1	1.25

Measurements of film cooling effectiveness and discharge coefficients

The tested surface temperature was measured by infrared thermography system and stored in the computer for subsequent data processing. The K-type thermocouples are placed

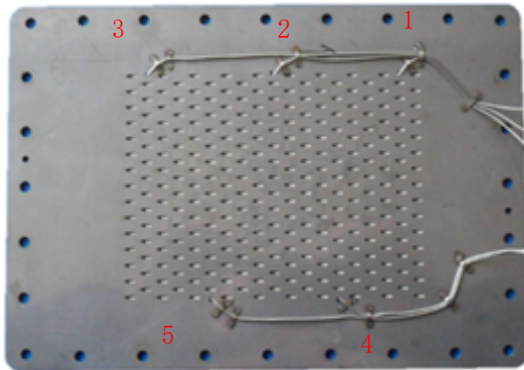


Figure 4. Thermocouples placed on the test plate

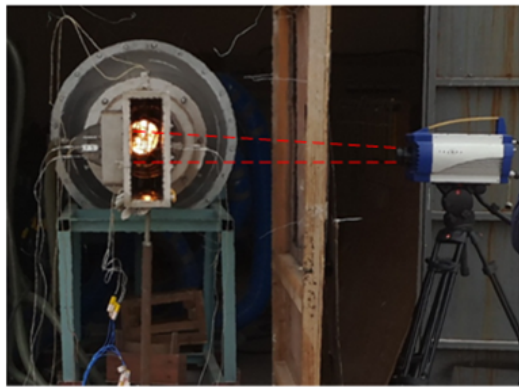


Figure 5. Infrared thermography system

deviation from the classic definition of the film cooling discharge coefficient, it is more convenient to compare with those of different film holes with the same entry cross-section and evaluate the effect of the film holes. The measurement P_C^* is coolant chamber total pressure and P_g is static pressure in the mainstream channel, this leads to:

$$C_D = \frac{m_{re}}{A_c \sqrt{2\rho(P_C^* - P_g)}} \quad (2)$$

Experimental uncertainties

Accounting for the individual uncertainties in setting the flow, the relative overall uncertainty in film-cooling effectiveness is estimated to be 3.23%. (The tested surface temperature error is less than 0.25%, the mainstream temperature error is 0.73% and radiation effects are found to be small, less than 1% effect on film-cooling effectiveness.)

Experimental results

Cooling effectiveness

The temperature data obtained by infrared thermography on the test surface range from the 20 mm upstream of the hole area, and all the hole area involved, which are shown as data extracted region in fig. 6. The cooling efficiency can be calculated according to the eq. (1).

on both sides of the hole region to reduce the effect to the flow and increase the accuracy of the temperature measurement, fig. 4. The surface which is the opposite of the test plate is equipped with infrared window that has highly transparent to infrared radiation, $\tau = 0.93$, in the wavelength range from $8 \mu\text{m}$ to $9 \mu\text{m}$. The radiation collected from the test plate is digitized into an array of 240×320 pixels.

The temperature distribution data obtained by infrared thermograph system, fig. 5, of test surface can be processed by MATLAB program. Thus, the film cooling effectiveness is described:

$$\eta = \frac{T_g - T_w}{T_g - T_c} \quad (1)$$

where the T_g is mainstream temperature, T_c – the coolant temperature and the T_w – the local surface temperature which is obtained by the infrared thermograph.

The discharge coefficient, C_D , is defined as the ratio of real and ideal mass-flow through the film hole. This definition uses the cross-section of the impingement hole entry, A_c , as the metering area. Although this is a

Although the present data is capable of revealing detailed distributions over the entire viewing domain, most local data are presented along streamwise paths for direct comparison. One of the paths is along the centerline of the film holes, which as the X -axis in the co-ordinate system, and the origin of X locates at the beginning of the data extracted region.

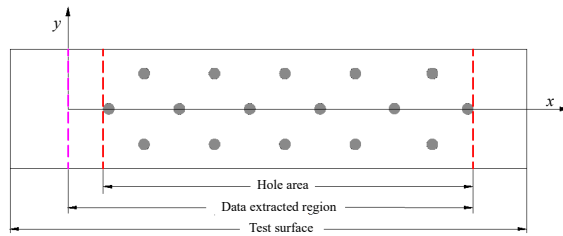


Figure 6. Range of data extracted region

The Y -axis is perpendicular to the X -axis, which is along the spanwise path. These line datas are good representatives of the transport features over the entire measurement domain, since the overall distributions in η are periodic across the span of the test surface. The case with $M = 2.2$ is presented in fig. 6.

Effect of film hole diameter

Figure 7 shows the cooling effectiveness distributions on the test surface under the blowing ratio of 2.2. It can be seen that with the increase of the hole diameters, the cooling efficiency has much more uniform distribution, and the cooling performance is strengthened obviously. The Configuration A, whose overall cooling efficiency is about 0.8, and there is almost no η reaches 0.9. However, when the diameters increase to 0.85 mm, the middle of the test surface region process the efficiency of 0.9. Particularly, the cooling efficiency is more than 0.9 when the film hole diameters increase to 1.05 mm and 1.25 mm. In order to observe the differ-

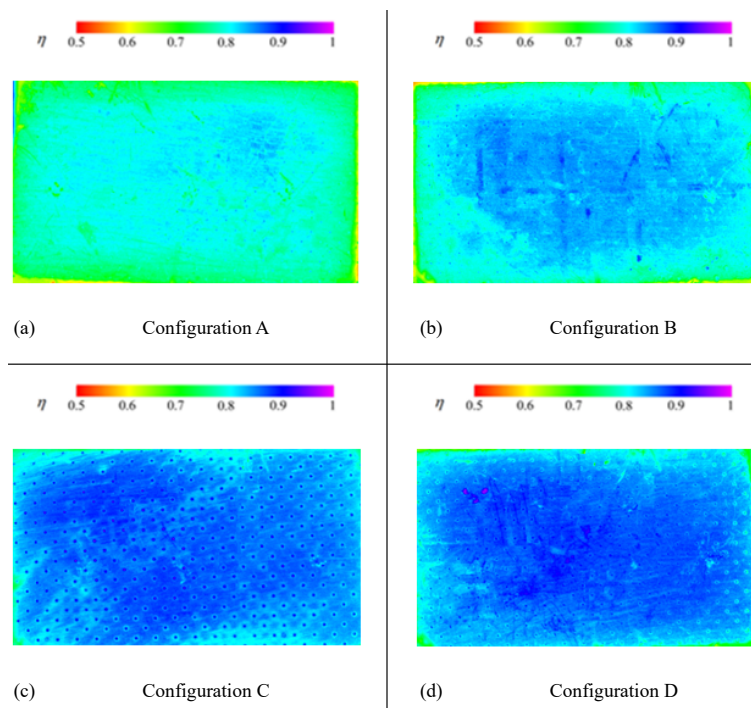


Figure 7. The film effectiveness distribution of test surface at $M = 2.2$

ences of the cooling efficiency in four film holes clearly. Figure 8 shows the streamwise cooling efficiency with different film holes, concretely, the centerline of the film holes defined in fig. 7. In fig. 8, the x/d represents the ratio of the distance along the X -axis to the hole diameter. It can be concluded that the cooling efficiency at the front end of the test surface (the range of 20 mm upstream of the hole area) is lower because the film has not formed. After the first row of holes, the efficiency increases gradually and presents the peak value in the film hole owing to the lower temperature of the hole surface. In addition, cooling efficiency fluctuations occur in the region between adjacent holes. Four configurations have same trend of efficiency distribution. Nevertheless, when the film hole diameters increase, the value of the cooling efficiency is increased and the fluctuation amplitude reduced.

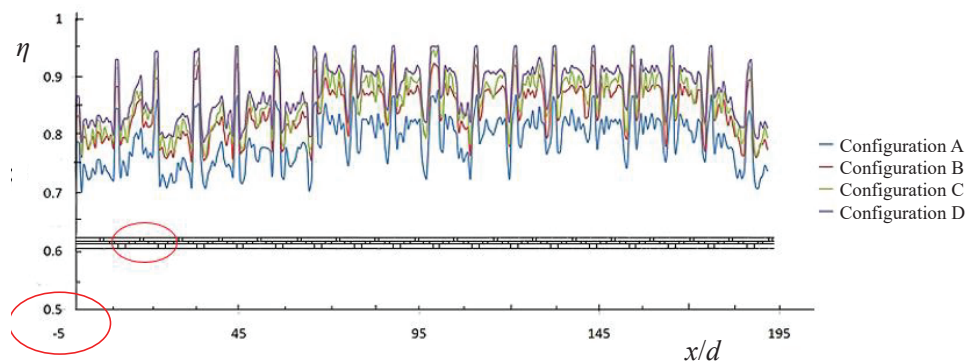


Figure 8. Streamwise distribution of film effectiveness at $M = 2.2$

Figure 9 shows the pressure distribution of the four models in the circle region in fig. 8. With the increase of the film hole diameters, the pressure on the inside of the target plate is increased owing to the jet flow from impingent hole and the impingent zone becomes larger. According to the analysis, the pressure drop on both sides of the lamilloy Δp can be described as the sum of the pressure difference on both sides of the impingement hole Δp_1 and the differ-

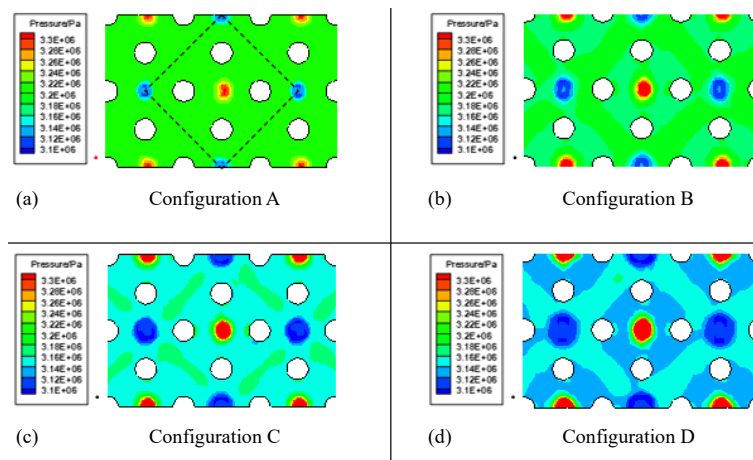


Figure 9. Pressure distribution on the inside of target plate of four models

ence of pressure on both sides of the film hole Δp_2 , that is $\Delta p = \Delta p_1 + \Delta p_2$. In this paper, the research on the effect of the film hole diameter is based on the condition that the pressure of the mainstream and the coolant is constant. So, when the film hole diameters increase, the flow resistance reduced on both sides of the film hole, which means the Δp_2 is decreased. Thus, the pressure drop Δp_1 is increased, resulting the pressure on the inside of the target plate is increased too, shown clearly in fig. 9. From the equation that $\Delta p_1 = \rho u^2/2$, the velocity of jet flow is increased, the impingement impact from the impingement plate was strengthened. The fig. 10 shows the velocity and heat transfer coefficients on the inside of target plate, it is obvious that the convective heat transfer on target plate and pin-fins, fig. 11, are strengthened too. Meanwhile, the spanwise distance downstream the film holes enlarged and the cooling efficiency grows higher.

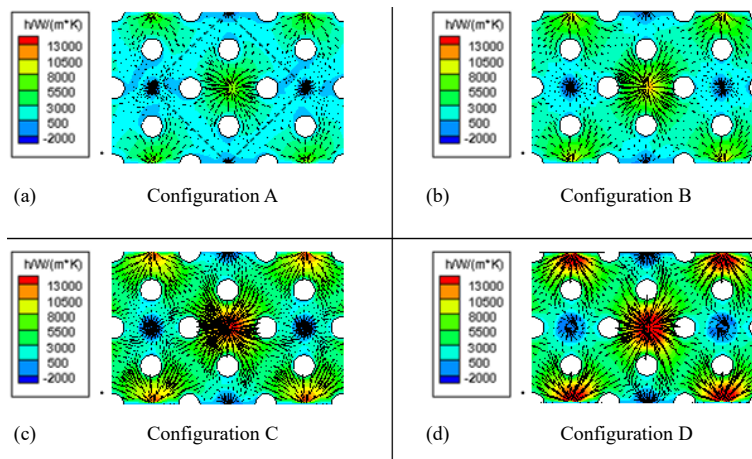


Figure 10. Velocity and heat transfer coefficient on the inside of target plate of four models

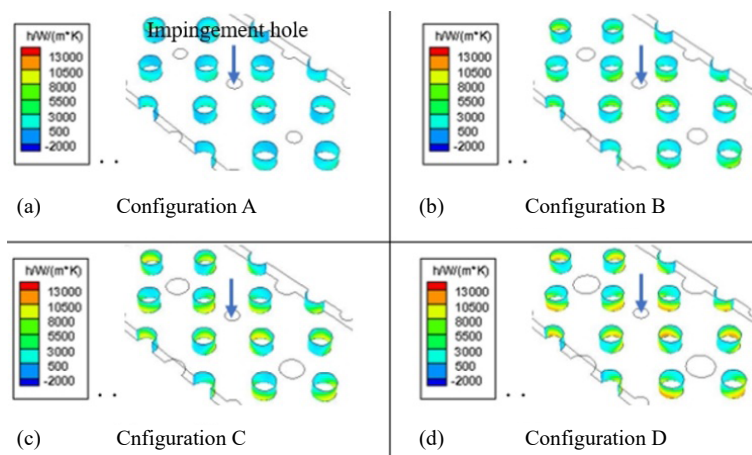


Figure 11. Heat transfer coefficient on the pin-fins of four models

Discharge coefficients

The discharge coefficients have been measured for all lamilloy configurations investigated. Figure 12 displays the discharge coefficients of the four film holes under six blowing ratios varying from 0.6 to 2.5, as the six group of lines shown, in which the four points represent the different film holes. Generally, the discharge coefficients increase with the blowing ratio increasing. For instance, the C_D of Configuration A is increasing from 0.62 to 0.675, which the rate of increase is 8.9%, and as the film hole diameter continues to increase, the C_D increase slightly with the blowing increased, only 3% growth rate of Configuration D. On the other hand, under the same blowing ratios, as the diameters of film hole increase, the discharge coefficients are increased equally. However, differences from configuration to configuration are rather small – typically less than 1% except for Configuration A, of which the C_D is a little lower than others' value.

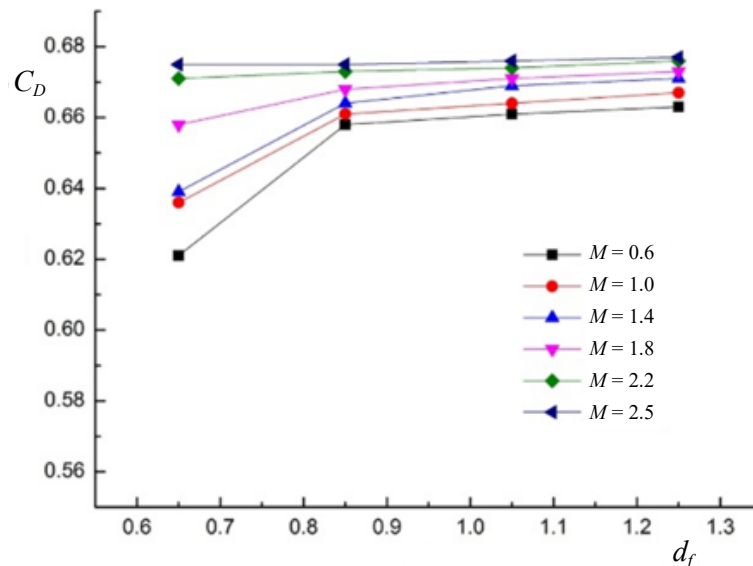


Figure 12. Discharge coefficients distribution of four configurations at different blowing ratio

Conclusions

Experimental investigations have been carried out on the impact of various film hole diameters and blowing ratios on the film-cooling effectiveness and discharge coefficient of lamilloy cooling structures. An infrared thermography measurement technique, which can process the initial wall temperature, is used to measure the wall temperature, and the discharge coefficients are obtained too. The main findings can be summarized as follows.

- When the film hole diameters increase, the impingement impact from the impingement plate was strengthened, and the heat transfer of the pin-fins increase too, and spanwise distance downstream the film holes enlarged in sequence.
- In the same lamilloy configuration, the cooling efficiency increases with the increasing blowing ratio, which caused by the increasing of impingement cooling effect and film cooling effectiveness. When blowing ratio reaches a higher value, the impingement cooling

effect continues to increase while the film begins to separate from the surface, resulting that the growth is slower.

- The discharge coefficient increases with diameter increasing, and which increase with flow ratio under same film hole diameter.

References

- [1] Ashmole, P. J., Rolls-Royce Limited, East Kilbride, Introduction the Rolls-Royce Tay, *Proceedings*, 19th Joint Propulsion Conference, Washington DC, 1983, 1-12
- [2] Nealy, D. A., Reider, S. B., Evaluation of Laminated Porous Wall Materials for Combustor Liner Cooling, *Journal of Engineering for Power*, 102 (1990), 2, pp. 269-276
- [3] Vajravelu, K., Li, R., Effects of Second - Order Slip and Drag Reduction in Boundary Layer Flows, *Applied Mathematics & Nonlinear Sciences*, 3 (2018), 1, pp. 291-302
- [4] Caraballo, T., et al., An Iterative Method for Non-Autonomous Nonlocal Reaction - Diffusion Equations, *Applied Mathematics & Nonlinear Sciences*, 2 (2017), 1, pp. 73-82
- [5] Wassell, A. B., Bhangu, J. K., The Development and Application of Improved Combustor Wall Cooling Techniques, *Proceedings*, Int. Gas Turbine Conf. and Products Show, New Orleans, La., USA, 1980, 80-GT-66
- [6] Sweeney, P. C., Rhodes, J. F., An Infrared Technique for Evaluating Turbine Airfoil Cooling Designs, *ASMS. Journal of Turbomachinery*, 122 (2001), 1, pp. 170-177
- [7] Kong, M. Z., et al., Research on Heat Transfer Characteristics of Lamilloy Internal Surfaces Using Transient Liquid Crystal Technique, *Journal of Aerospace Power*, 24 (2009), 2, pp. 340-346
- [8] Funazaki, K., et al., Heat Transfer Characteristics of an Integrated Cooling Configuration of Ultra-High Temperature Turbine Blades, Experimental and Numerical Investigations, *Proceedings*, Power for Land, Sea, and Air, New Orleans, La., USA, 2001
- [9] Funazaki, K., Hachlya, K., Systematic Numerical Studies on Heat Transfer and Aerodynamic Characteristics of Impingement Cooling Devices Combined with Pins, *Proceedings*, Int. Joint Power Generation Conf., Atlanta, Geo., USA, 2003, pp. 185-192
- [10] Wu, H. L., Peng, X. F., Transpiration Cooling Using Porous Triple-Laminated Plates, *Proceedings*, ASME 2003 Heat Transfer Summer Conference, Las Vegas, Nev., USA, 2003, pp. 735-740
- [11] Zhang, B., et al., Numerical Investigation of Flow and Heat Transfer Characteristics in Plate with Multiple Incline Stage Holes, *Tehnicki Vjesnik*, 26 (2019), 2, pp. 471-477
- [12] Andrews, G. E., Hussain, C. I. Enhanced Impingement Heat Transfer: The Influence of Impingement X/D for Interrupted Rib Obstacles (Rectangular Pin Fins), *Journal of Turbomachinery*, 128 (2006), 2, pp. 321-331